How cations determine the interfacial potential profile: relevance for the CO_2 reduction reaction

Ghulam Hussain,[†a,b,1] Laura Pérez-Martínez,[†a] Jia-Bo Le,[†c] Marco Papasizza,[a] Gema Cabello,[a,d,2] Jun Cheng[c] and Angel Cuesta[a]*

[a]*School of Natural and Computing Sciences, University of Aberdeen, Aberdeen AB24 3UE, Scotland, UK.*

[b]*Curtin Institute for Functional Molecules and Interfaces, School of Molecular and Life Sciences, Curtin University, GPO Box U1987, Perth, 6845, WA, Australia.*

[c]*State Key Laboratory of Physical Chemistry of Solid Surfaces, iChEM, College of Chemistry and Chemical Engineering, Xiamen University, Xiamen 361005, China*

[d]*School of Medicine, Medical Sciences and Nutrition, University of Aberdeen, Foresterhill, Aberdeen AB25 2ZD, Scotland, UK.*

[1]Current address: University of Education, Division of Science and Technology, Department of Chemistry, College Road, Township, Lahore, Punjab, Pakistan

[2]Current address: Living Systems Institute, Department of Physics and Astronomy, University of Exeter, Stocker Road, Exeter EX4 4QD, UK.

[†] G.H., L.P.-M. and J.L. contributed equally to this work.

*Corresponding author: angel.cuestaciscar@abdn.ac.uk

ABSTRACT

The strong effect of the electrolyte cation on the activity and selectivity of the CO_2 reduction reaction (CO_2RR) can only be understood and controlled if the cation's effect on the interfacial potential distribution is known. Using CO (the key intermediate in the CO_2RR) adsorbed on Pt as a probe molecule, and combining IR spectroscopy, capacitance measurements and ab initio molecular dynamics, we show that the cation size determines the location of the outer Helmholtz plane, whereby smaller cations increase not just the polarisation but, most importantly, the polarizability of adsorbed CO (CO_{ad}) and the accumulation of electronic density on the oxygen atom of CO_{ad}. This strongly affects its adsorption energy, the degree of hydrogen bonding of interfacial water to CO_{ad} and the degree of polarisation of water molecules in the cation's solvation shell, all of which can deeply affect the subsequent steps of the CO_2RR.

Keywords: double-layer structure; cation effects; CO_2 reduction reaction; adsorbed CO; vibrational Stark effect

1. Introduction

Electrochemistry is central to a multitude of technologically relevant processes. The essential event in any electrochemical process is the electron transfer across the interface between two heterogeneous media. The microscopic structure of the electric double layer (EDL) plays, therefore, a critical role in determining the rate and selectivity of electrochemical reactions. Particularly, the potential profile across the interface is of the utmost importance, because it can affect the stability of adsorbed intermediates[1–3] or polarise molecules within the EDL [4,5].

The effect of the electrolyte cation on the efficiency and selectivity of the CO_2 reduction reaction (CO_2RR) was discovered by Hori and co-workers [6], although the effect of cations on the kinetics of electrochemical reduction reactions had been known since Frumkin's

pioneering work in the 1930's [7]. The dependence of the location of the outer Helmholtz plane (OHP) on the size of the hydrated cation has been identified as one of its main causes [8–10].

Singh et al. [4] have recently suggested that the pK_a of cation hydrolysis at the EDL differs from that in the bulk, due to the polarisation of water molecules in the cation's hydration shell, which results in cation-dependent interfacial buffering capacities. As the activity and selectivity of the CO_2RR are pH dependent [11–13], this could explain the cation effect on this reaction. Our group [5] later provided spectroscopic evidence that the pH increase at the interface during the CO_2RR in CO_2-saturated bicarbonate buffers is indeed cation dependent. Perez-Gallent et al. [14] have also recently shown that adsorbed COCOH (the likely intermediate in the formation of C_2 products) is better stabilised in the presence of Li^+, Na^+ or K^+ than with Rb^+ or Cs^+. Although differing in the details, the interpretations of both Singh et al. [4] and Pérez-Gallent et al. [14] rest both on cation-induced differences in the electric field at the EDL. An in principle alternative explanation was proposed very recently by Li et al. [15], who suggested that the degree of hydrogen bonding of interfacial water to adsorbed CO (CO_{ad}) is cation dependent, but did not discuss how and why different cations leed to different degrees of hydrogen bonding of interfacial water to surface species. As we will show in this contribution, this is also a consequence of cation-induced differences in the electric field at the EDL.

CO-terminated Pt electrodes are an excellent platform to investigate double layer effects. They have been very well characterised spectroscopically and electrochemically [16–24]. CO adsorbs strongly on Pt, remains in the same structure over a wide potential range, and blocks the specific adsorption of ions on the electrode surface. These characteristics also make it most suitable for first-principles calculations. Furthermore, CO_{ad} is an intermediate in the reduction of CO_2 to hydrocarbons [25–27], and evidence of a cation effect on its stability or

on its interaction with interfacial water has therefore direct relevance to understanding the CO_2RR. Recently, Koper and co-workers [23,24] have shown that both the interfacial capacitance and the dependence of the C-O stretching frequency of a CO-terminated Pt electrode on the potential ($\frac{\partial \bar{\nu}_{CO_L}}{\partial \Delta\phi}$, often called the Stark tuning rate, STR) are independent of the concentration of the supporting electrolyte for concentrations above 10^{-3} mol L^{-1}. This implies that the interfacial capacitance is dominated by that of the Helmholtz layer (so-called Helmholtz capacitance, C_H), which must be determined by the location of the OHP and, therefore, CO-terminated Pt electrodes offer an ideal platform to explore the consequences of a cation-dependent location of the OHP.

Here, we combine surface-enhanced infrared absorption spectroscopy in the attenuated total reflection mode (ATR-SEIRAS) and capacitance measurements to show that the size of the hydrated cation determines the interfacial potential profile. We develop a theoretical formulation that explains the experimental observations and is supported by ab-initio molecular dynamics (AIMD) simulations, and identify the key effects, all of them due to cation-induced differences in the electric field at the EDL, that combine and reinforce each other to yield the strong cation sensitivity of the CO_2RR. An adequate control of the delicate balance between these three effects should lead to a better control of the activity and selectivity of this extremely important reaction.

2. Experimental

2.1. Materials. The working electrode was a Pt film deposited on the totally reflecting plane of a Si prism bevelled at 60º, following a procedure reported elsewhere [28]. The Pt-covered Si prism was attached to the spectroelectrochemical cell using an O-ring seal. Electrical contact to the film was made by pressing onto it a circular platinum wire. Prior to any IR measurements, the electrode was cycled repetitively in 0.1 M $HClO_4$. The cell was then rinsed thoroughly with Ultrapure water (Milli-Q) and fill with the desired electrolyte. A

Ag/AgCl (KCl_{sat}) electrode was used as reference, but all the potentials in the text are referred to the SHE. The counter electrode was a flame-annealed Pt wire.

Electrolytes were prepared dissolving $HClO_4$ (70%, Merck p.a.), H_2SO_4 (96%, Merck Suprapur), $LiClO_4$ (Aldrich, 99.99% trace metals basis), $NaClO_4$ (Fluka for HPLC, ≥ 99.0%), K_2SO_4 (Aldrich, 99.99% trace metals basis), Rb_2SO_4 (Aldrich 99.8% trace metals basis), $CsClO_4$ (Aldrich, 99.995% trace metals basis), $MgSO_4{\cdot}7H_2O$ (Sigma BioUltra ≥ 99.5%), $Sr(ClO_4)_2{\cdot}3H_2O$ (Alfa Aesar 98%), $Ca(ClO_4)_2{\cdot}4H_2O$ (Aldrich 99%), $(NH_4)_2SO_4$ (Aldrich 9.999% trace metals basis), $[N(CH_3)_4]ClO_4$ (Acros Organics 98%), $[N(CH_2CH_3)_4]BF_4$ (Sigma-Aldrich for electrochemical analysis, ≥ 99.0%), $[N((CH_2)_2CH_3)_4]ClO_4$ (Acros Organics 98%) or $[N((CH_2)_3CH_3)_4]ClO_4$ (Sigma-Aldrich for electrochemical analysis, ≥ 99.0%) in ultrapure water (MilliQ). All solutions were prepared to a concentration 0.1 M except in the case of $[N(CH_2CH_3)_4]BF_4$, for which a concentration of 0.01 M was used. In order to confirm that the lower concentration does not affect either C_T or $\frac{d\bar{\nu}}{d\Delta\phi}$ experiments were also performed with a 10^{-3} M concentration of $[N(CH_2CH_3)_4]BF_4$, and the same values were obtained for both magnitudes. As the potential region of stability of CO_{ad} is much more negative than the potential of zero charge (pzc) of a CO-covered Pt electrode (1.10 V vs. SHE for Pt(111)[18]), we do not expect the nature of the anion to have any effect on the spectra or, in general, the interfacial structure and properties. For H^+, both H_2SO_4 and $HClO_4$ yielded the same results.

The electrolyte was saturated with research grade carbon monoxide (99.9995 % purity from BOC) for 30 minutes before every experiment, and CO was bubbled through the electrolyte throughout the experiment.

2.2. Experimental Methods. ATR-SEIRA spectra were recorded using a Nicolet iS50R FTIR spectrometer equipped with an MCT detector and a home- made ATR accessory, using unpolarized light. Differential spectra are reported in absorbance units, calculated as

$-\log(R_{sample}/R_{reference})$, where $R_{reference}$ and R_{sample} are the reference and sample spectra, respectively. Positive bands corresponds to species present (or at higher concentration) in the sample spectrum that were absent (or at lower concentration) in the background spectrum, while negative bands correspond to species present (or at higher concentration) in the background spectrum that are absent (or at lower concentration) in the sample spectrum. Potential-step differential spectra were obtained by accumulating 100 interferograms with a resolution of 4 cm^{-1}. The electrode potential was controlled with an EmStat3 mini USB potentiostat (PalmSens).

The interfacial capacitance of a CO-covered Pt electrode in the different electrolytes was recorded by cycling the potential of a polycrystalline Pt electrode between 0.1 and 0.4 V at 0.05 V s^{-1}. The capacitance was obtained by dividing the current density (which is constant within this potential range) by the scan rate.

2.3. Computational methods. The CO-covered Pt(111) surface was modelled using a $p(4 \times 4)$ periodic slab of 4 layers of Pt atoms. Based on the experimental results, the total surface CO coverage is set to be 3/4 ML (2 x 2 arrangement), with 1/4 ML CO on top sites and 1/2 ML on three-fold hollow sites. The box size of the simulation model is 11.246 x 11.246 x 40 $Å^3$, and three dimensional periodic boundary condition is applied. Then, the vacuum space between the geometrically-optimized Pt(111)-CO surface and its images is fully filled with water molecules. This model replicates the PZC condition of the Pt(111)-CO/water interface.

The electric double layers are modelled by inserting Na atoms at ~3 Å away from the surface in the Pt(111)-CO/water interface. As expected, Na atoms are spontaneously oxidized to Na^+ in liquid water. As the whole interface has to be neutral, a charge identical in magnitude but of opposite sign to that of the Na^+ ions emerges on the Fermi level of the Pt(111)-CO surface. The charge density (σ) on the Pt(111)-CO surface is therefore

determined by the number of Na atoms inserted in the simulation cell. In this work, we have modelled three Pt(111)-CO/water interfaces: σ = 0, -14.6 and -29.2 μC cm^{-2}.

The DFT implemented in CP2K is based on a hybrid Gaussian plane wave (GPW) scheme, the orbitals are described by an atom-centred Gaussian-type basis set, and an auxiliary plane wave basis set is used to re-expand the electron density in the reciprocal space. The 2s, 2p electrons of O, 2s, 2p electrons of C, 2s, 2p, 3s electrons of Na, and 5d, 6s electrons of Pt are treated as valence, the rest core electrons are represented by Goedecker-Teter-Hutter (GTH) pseudopotentials. The Gaussian basis set is double-ζ with one set of polarization functions (DZVP), and the energy cut-off is set to 400 Ry. We employ BLYP functional to describe the exchange-correlation effects, and the dispersion correction is applied in all calculations with the Grimme D3 method. The second-generation Car-Parrinello molecular dynamics is used for the DFTMD simulation, and the target temperature is set to 330 K. The discretized integration step is 0.5 fs, with $\gamma L = 0.001$ fs^{-1}. The first 2 ps of the simulation trajectory was regarded as the equilibration period, then followed by a production period of 15∼20 ps. Due to the large size of the cell, only the Γ point in reciprocal space was used. To obtain the vibrational density of states (VDOS) spectra of CO, the velocity-velocity autocorrelation function is used.

3. Results and discussion

We use ATR-SEIRAS to analyse cation effects on the C-O and O-H stretching modes of CO_{ad} and of interfacial water, respectively, in CO-saturated solutions. ATR-SEIRAS (Fig. 1a) combines the ATR geometry with the short range of the SEIRA effect for improved interfacial sensitivity [29,30]. A deeper insight into the EDL structure was reached with AIMD simulations making use of the computational standard hydrogen electrode (SHE) [31]. Figure 1b illustrates the model of the Pt(111)-CO/water interface used for AIMD simulations.

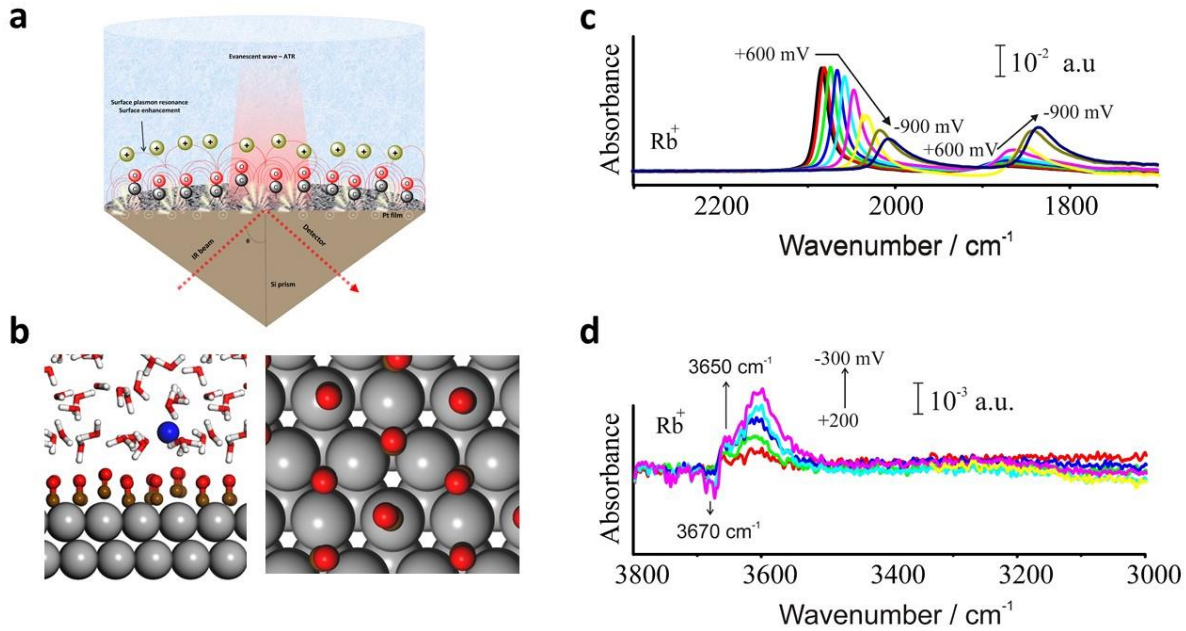

Figure 1. (a) Schematic illustration of the surface sensitivity of surface-enhanced infrared absorption spectroscopy in the attenuated total reflection mode (ATR-SEIRAS), due to the combination of the thin layer of electrolyte probed by the evanescent wave (typical of the ATR configuration) and to the short rage of the SEIRA effect generated by surface plasmon excitation within the rough metal film deposited on the Si prismatic window. **(b)** Model of the Pt(111)-CO/water interface used for AIMD simulations. Pt, C, O, H and cation are coloured by grey, brown, red, white and blue, respectively. The Pt(111) surface is covered by the (2 x 2)-3CO structure (θ = 0.75 ML) known to exist on this surface in CO-saturated solutions at $E \leq 0.45$ V *vs.* RHE [32]. **(c)** ATR-SEIRA spectra of a Pt electrode in CO-saturated 0.1 M Rb_2SO_4 in the spectral region corresponding to the C-O stretching of adsorbed CO. The spectra are shown at potential intervals of 0.20 V for the sake of clarity and were calculated using the spectrum of the CO-free Pt surface at the open-circuit potential as background. **(d)** ATR-SEIRA spectra of a Pt electrode in CO-saturated 0.1 M Rb_2SO_4 in the spectral region corresponding to the O-H stretching of H_2O. The spectra are show at potential intervals of 100 mV for the sake of clarity and were calculated using the spectrum of CO-covered Pt surface at +0.4 V as background**.**

Experiments were performed with 14 different cations: H^+, NH_4^+, Li^+, Na^+, K^+, Rb^+, Cs^+, Mg^{2+}, Ca^{2+}, Sr^{2+}, tetramethylammonium (TMA^+), tetraethylammonium (TEA^+), tetrapropylammonium (TPA^+) and tetrabutylammonium (TBA^+). Figs. 1c and d show the

spectra obtained with Rb^+ in the CO and OH stretching regions, respectively. Spectra for all the cations can be found in Fig. S1.

3.1. Cation effect on the potential dependence of $\bar{\nu}_{\mathrm{CO_L}}$ and on C_T: EDL model. In the CO stretching region, all the spectra consist of two bands that red-shift with increasingly negative potential (Fig. 1c and Fig. S1a). The band between ca. 2000 and ca. 2090 cm^{-1} corresponds to linearly adsorbed CO (CO_L), while the band between 1800 and 1900 cm^{-1} corresponds to bridge-bonded adsorbed CO (CO_B). The dependence of the CO_L frequency ($\bar{\nu}_{\mathrm{CO_L}}$) on potential is shown in Fig. 2a. There is a wide potential region of linear dependence (shown in more detail in Fig. S2). The deviation from linearity at negative potentials is not central to this discussion and is explained in more detail in the Supporting Information (SI). We will focus our discussion on CO_L. CO_B shows a similar dependence on potential, but the bands are broader, and a detailed analysis is subject to a larger error.

The STR can be expressed as:

$$\frac{\partial \bar{\nu}_{\mathrm{CO_L}}}{\partial \Delta\phi} = \frac{\partial \bar{\nu}_{\mathrm{CO_L}}}{\partial F}\frac{\partial F}{\partial \Delta\phi} \qquad \text{Eq. 1}$$

where, in a first approximation, $\frac{\partial \bar{\nu}_{\mathrm{CO_L}}}{\partial F}$ can be considered as constant. As the interfacial electric field is $F = \frac{\Delta\phi}{\Delta x_{\mathrm{dl}}}$, where Δx_{dl} is the thickness of the EDL, $\frac{\partial F}{\partial \Delta\phi} = \frac{1}{\Delta x_{\mathrm{dl}}}$. Therefore, assuming that Δx_{dl} is determined by the size of the cation, a direct proportionality between the STR and the inverse of the cation radius should be obtained. Fig. 2c shows a plot of the STR (in the region of linear dependence between $\bar{\nu}_{\mathrm{CO_L}}$ and the potential) *vs.* the charge number to hydrodynamic radius ratio (*i.e.*, the radius of the cation plus its hydration shell). The latter was calculated from the cation's limiting molar conductivity, λ (see SI). Similar cation effects on the STR have been found by Roth and Weaver [16] for CO_{ad} on Pt in non-aqueous media, and have also been recently reported for CO_{ad} on Cu [15,33]. The values of the STR for all the cations used in this study are provided in Table S1. The value obtained for H^+ is in

good agreement with literature values for polycrystalline Pt [34]. Although a reasonable direct proportionality is obtained as the cation size decreases from aqueous TBA^+ to aqueous Li^+, for smaller cations ($\frac{z}{r_H} > 4.5 \times 10^{-3}$) there is a clear deviation from the expected behaviour.

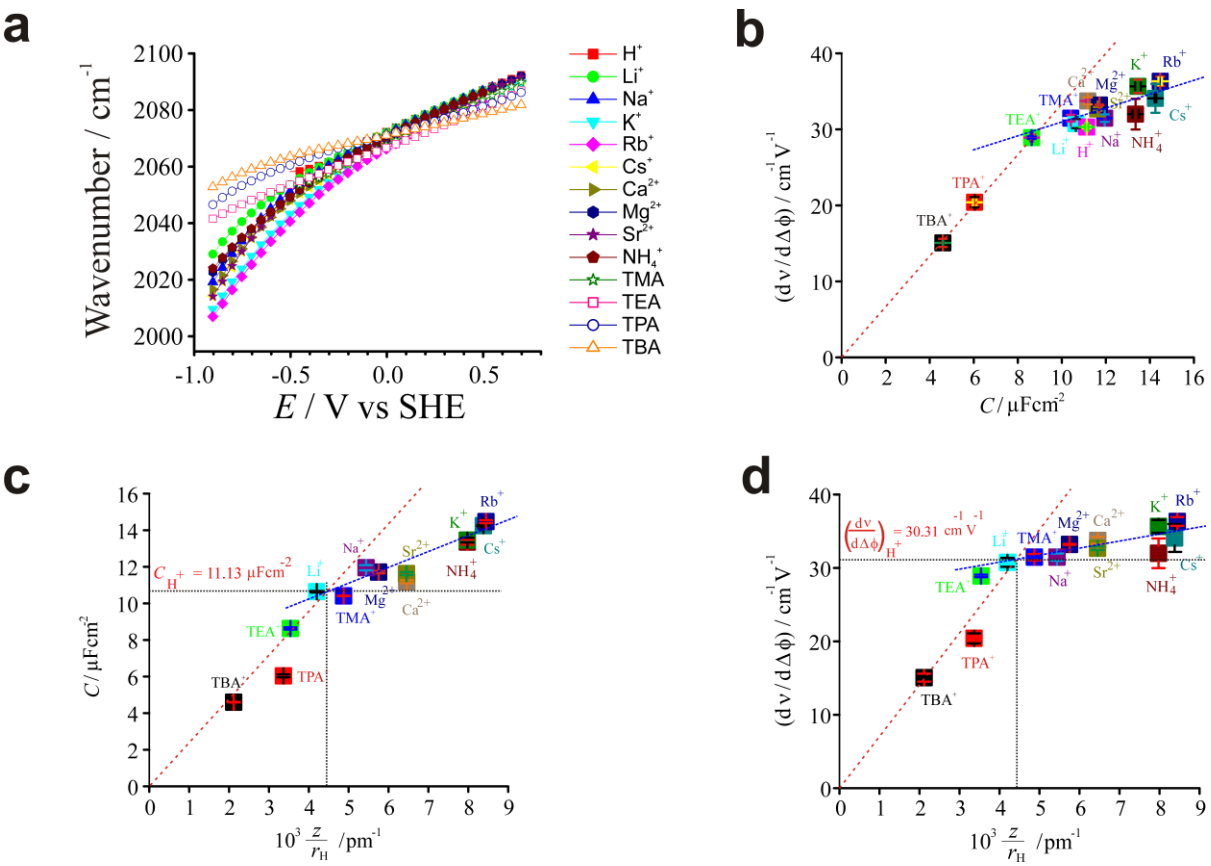

Figure 2. (a) Plot of the CO_L stretching frequency as a function of the electrode potential for all the cations used in this study. **(b)** Plot of the Stark tuning rate *vs.* the interfacial capacitance for all 14 cations used in this study. The dashed red line is the best linear fit to the data corresponding to the three largest cations (TBA^+, TPA^+ and TEA^+). The dashed blue line is a linear fit to the rest of the data. **(c)** and **(d)**, Plots of the interfacial capacitance and the Stark tuning rate, respectively, as a function of the ratio between the charge number of the cation and the cation's hydrodynamic radius, $\frac{z}{r_H}$, as obtained from the corresponding limiting ionic conductivity, λ. The dashed horizontal lines in **c** and **d** correspond to the interfacial capacitance and the Stark tuning rate, respectively, when H^+ is the electrolyte cation, and the vertical dashed lines correspond to the resulting estimated effective radius of hydrated H^+ at the electrical double layer.

A similar deviation from the expected behaviour is observed for the interfacial capacitance, as, in the simplest possible model of the EDL, $C_{\mathrm{H}} = \frac{\varepsilon\varepsilon_{\mathrm{o}}}{\Delta x_{\mathrm{dl}}}$, with ε_{o} the vacuum permittivity and ε the dielectric constant of the interfacial region As shown in Fig. 2d, a reasonable direct proportionality is obtained again only for cations larger than aqueous Li^+. The values of C_{T} for all the cations used in this study are reported in Table S1.

Please note that, due to proton hopping between water molecules [35], the size of hydrated H^+ cannot be determined from λ, and H^+ has therefore not been included in Figs. 2c and d. However, these figures allow for an estimation of the effective size of hydrated H^+ of approximately 2.2 Å. It is also worth noting that both the STR and C_{H} show a good correlation, not with the radius of the cation, but with $\frac{z}{r_{\mathrm{H}}}$. In other words, the ratio between the cation's charge and its hydrodynamic radius behaves as the effective cation size. This has to be due to the fact that the potential generated by a central ion decays with the distance from the ion, r, as $\frac{z}{r}$ and, consequently, a monovalent ion with a hydrodynamic radius r_{H} and a divalent ion with a hydrodynamic radius $2r_{\mathrm{H}}$ will induce exactly the same potential at the surface of the solvation shell, leading to the same C_{T} and the same STR, as found experimentally (Figs. 2c and d). This also implies that the potential drop across the cation's hydration shell contributes to the overall interfacial potential drop and must be taken into account when describing the structure of the EDL.

AIMD simulations offer a deeper insight into the EDL structure. We first calculate the electrode potential at different surface charge densities (σ). Computing costs limit our calculations to Na^+ and to σ = 0, -14.6 and -29.2 μC cm^{-2}, corresponding to 0, 1 or 2 Na^+ ions in the simulation cell, respectively. The computed pzc of the Pt(111)-CO/water interface is ~1.1 V vs SHE (Fig. 3a, inset), in good agreement with the experimental value [18]. The computed C_{T} is 13 μF cm^{-2} (Fig. 3a, inset), also in good agreement with the experimental

result for Na^+ (Table S1). Computed IR spectra of the (2 x 2) structure of CO on Pt(111) can be found in the SI (Fig. S3), and yield a computed STR of 40 cm^{-1} V^{-1} for CO_L, in reasonable agreement with experimental values in this work and elsewhere [20,36,37]. In summary, our AIMD simulation captures well the structure and properties of the EDL. At the pzc, the surface water is approximately 6 Å away from the Pt(111) surface and ~2 Å away from the oxygen atom of CO_{ad}, and shows a negligible degree of dipole orientation (Fig. 3a), in agreement with previous work with this and other surfaces [18,31]. At negative charge densities, water approaches closer to the electrode and orients with H pointing towards the surface (Fig. 3a, c, and d).

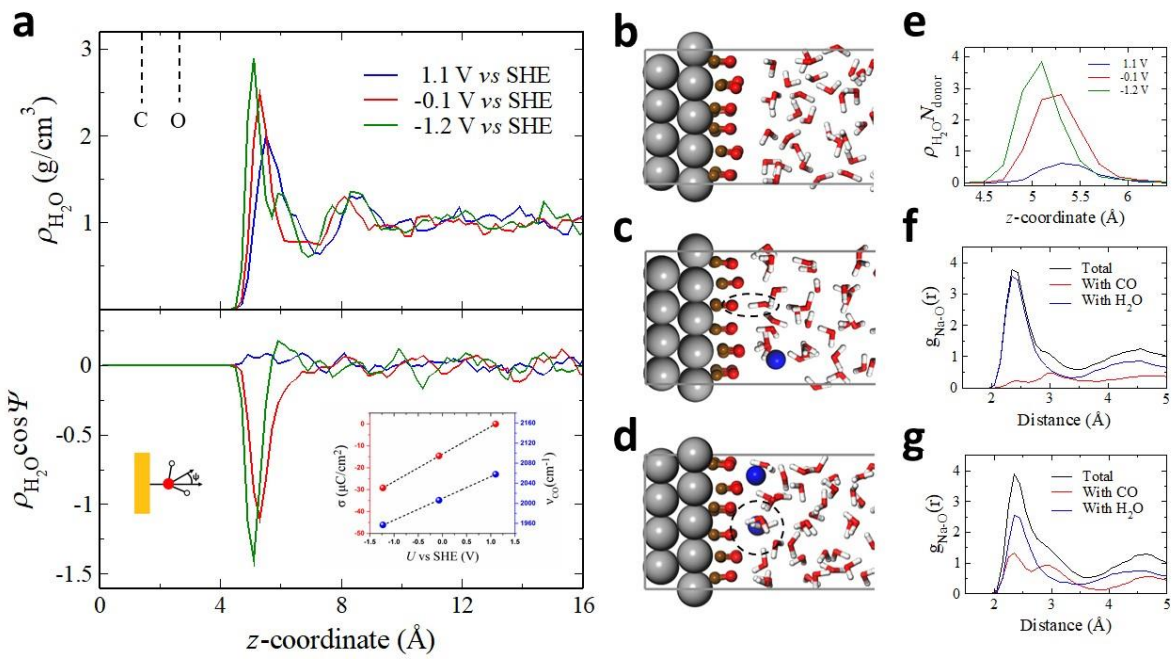

Figure 3. (a) Water density (ρ_{H_2O}, upper panel) and dipole orientation ($\rho_{H_2O}\cos\Psi$, lower panel) distributions along the surface normal direction (z-coordinate) at the pzc (+1.1 V), -0.1 V and -1.2 V. Zero in the z-coordinate axis corresponds to the Pt(111) surface, and the averaged positions of the C and O atoms of adsorbed CO have been labelled. The inset shows the surface charge density on the CO-covered Pt(111) electrode (σ) and the vibrational frequency of CO_L (ν_{CO}) at three different potentials, from which a pzc of +1.1 V and a capacitance of 13 μF cm^{-2} results. **(b)**, **(c)** and **(d)** show representative snapshots from AIMD at the pzc (+1.1 V), -0.1 V and -1.2 V, respectively. **(e)** Number of hydrogen bonds ($\rho_{H_2O}N_{donor}$) formed between CO and water along the z-coordinate at the pzc (+1.1 V), -0.1 V and -1.2 V, averaged in the XY plane. **(f)** and **(g)** show the distribution of

radial distances between Na^+ and O at -0.1 and -1.2 V vs SHE, respectively. The blue and red lines indicate the coordination of Na^+ with H_2O and CO, respectively, and the black line corresponds to the total number of oxygen atoms coordinated to Na^+.

Fig. 4 shows a model of the EDL which accounts for the experimental observations (Fig. 4a), the AIMD distribution of charge density (Fig. 4b) and the AIMD potential profile (Fig 4c). Fig. 4a takes into account that the effective radius of a cation at the interface is given by $r_{\mathrm{eff}} = \frac{r_{\mathrm{H}}}{z}$, as suggested by Figs. 2c and d and discussed above. At the pzc, the potential drop across the interface is small, but not zero. At -0.1 and -1.2 V the potential drop has three contributions (Figs. 4a and c), corresponding to (i) the CO adlayer, (ii) the ca. 2 Å wide gap between the electrode surface and interfacial water and (iii) the slice of interfacial water up to the OHP. The accumulation of electronic density on the oxygen atom of CO_{ad} at -0.1 and, particularly, -1.2 V, is clear in Fig. 4b. This is equivalent with having three capacitors in series, corresponding to the capacitance of the CO adlayer ($C_{\mathrm{a}} = \frac{\varepsilon_0 \varepsilon_{\mathrm{a}}}{\Delta x_{\mathrm{a}}}$), the capacitance of the gap ($C_{\mathrm{g}} = \frac{\varepsilon_0 \varepsilon_{\mathrm{g}}}{\Delta x_{\mathrm{g}}}$) and the capacitance of the water layer between the gap and the OHP ($C_{\mathrm{w}} = \frac{\varepsilon_0 \varepsilon_{\mathrm{w}}}{r_{\mathrm{eff}}}$), where ε_{a}, ε_{g} and ε_{w} are the dielectric constants of the CO adlayer, the gap and the water layer, respectively, and Δx_{a} and Δx_{g} are the thicknesses of the CO adlayer and the gap, respectively. *I.e.*, within this picture, C_{T} is given by:

$$C_{\mathrm{T}} \approx \frac{1}{C_{\mathrm{H}}} = \frac{1}{C_{\mathrm{a}}} + \frac{1}{C_{\mathrm{g}}} + \frac{1}{C_{\mathrm{w}}} = \frac{\varepsilon_0 \varepsilon_{\mathrm{a}} \varepsilon_{\mathrm{g}} \varepsilon_{\mathrm{w}}}{\varepsilon_{\mathrm{g}} \varepsilon_{\mathrm{w}} \Delta x_{\mathrm{a}} + \varepsilon_{\mathrm{a}} \varepsilon_{\mathrm{w}} \Delta x_{\mathrm{g}} + \varepsilon_{\mathrm{a}} \varepsilon_{\mathrm{g}} r_{\mathrm{eff}}} \qquad \text{Eq. 2}$$

The fraction of the potential drop falling within the CO adlayer will be given by $\frac{\Delta\phi_{\mathrm{a}}}{\Delta\phi} = \frac{C_{\mathrm{T}}}{C_{\mathrm{a}}}$ (similarly, the fractions of the potential drop corresponding to the gap and the interfacial water layer will be given by $\frac{\Delta\phi_{\mathrm{g}}}{\Delta\phi} = \frac{C_{\mathrm{T}}}{C_{\mathrm{g}}}$ and $\frac{\Delta\phi_{\mathrm{w}}}{\Delta\phi} = \frac{C_{\mathrm{T}}}{C_{\mathrm{w}}}$, respectively). The CO_{ad} stretching frequency is determined by the potential drop across the CO adlayer, $\Delta\phi_{\mathrm{a}}$, or, equivalently, by the electric field felt by the CO adlayer, $F_{\mathrm{a}} = \frac{\Delta\phi_{\mathrm{a}}}{\Delta x_{\mathrm{a}}}$. Accordingly:

$$\frac{\partial \bar{\nu}_{\mathrm{CO_L}}}{\partial \Delta\phi} = \frac{\partial \bar{\nu}_{\mathrm{CO_L}}}{\partial F_{\mathrm{a}}} \frac{\partial F_{\mathrm{a}}}{\partial \Delta\phi_{\mathrm{a}}} \frac{\partial \Delta\phi_{\mathrm{a}}}{\partial \Delta\phi} = \frac{\varepsilon_{\mathrm{g}}\varepsilon_{\mathrm{w}}}{\varepsilon_{\mathrm{g}}\varepsilon_{\mathrm{w}}\Delta x_{\mathrm{a}} + \varepsilon_{\mathrm{a}}\varepsilon_{\mathrm{w}}\Delta x_{\mathrm{g}} + \varepsilon_{\mathrm{a}}\varepsilon_{\mathrm{g}} r_{\mathrm{eff}}} \frac{\partial \bar{\nu}_{\mathrm{CO_L}}}{\partial F} = \frac{1}{\varepsilon_{\mathrm{o}}\varepsilon_{\mathrm{a}}} \frac{\partial \bar{\nu}_{\mathrm{CO_L}}}{\partial F} C_{\mathrm{T}} \qquad \text{Eq. 3}$$

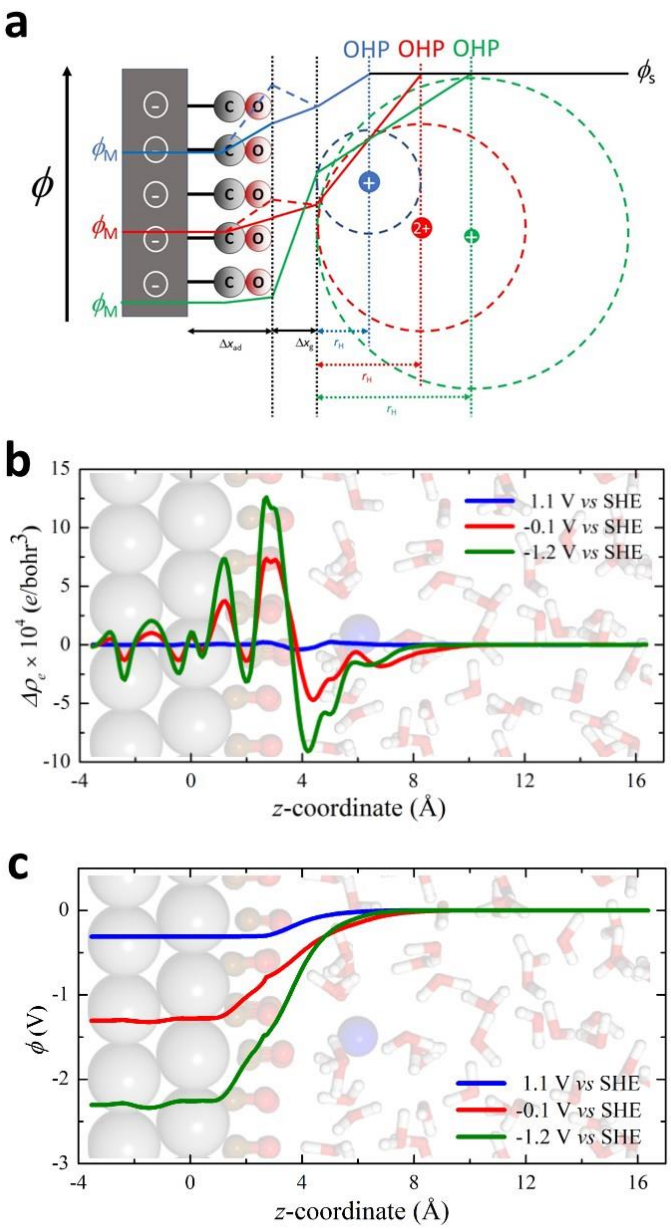

Figure 4. (a) Model illustrating the potential profile across the electrode-electrolyte interface, and the effect of the cation size on the interfacial properties and on the polarisation of the CO adlayer. The red cation is divalent, and therefore the situation depicted corresponds to twice the charge density than in the case of the monovalent blue and green cations. Δx_{a} and Δx_{g} correspond to the thickness of the CO adlayer and the vacuum gap, respectively, and r_{H} is the radius of the hydrated cation. The dashed lines illustrate the potential drops across the CO adlayer and the vacuum gap had ε_{a} remained constant. **(b)** Distribution of excess electronic density along the surface normal direction, as calculated from AIMD simulation and averaged in the XY plane. The excess

electronic density is defined as $\Delta\rho_e = \rho_{interface} - \rho_{Pt} - \rho_{water} - \rho_{Na}$. **(c)** Potential distribution across the interface. The zero *z*-coordinate corresponds to the Pt(111) surface. Blue, red and green curves correspond to the interface at the pzc (+1.1), -0.1 V and -1.2 V, respectively.

The clear direct proportionality between C_T and $\frac{z}{r_H}$ for $\frac{z}{r_H} < 4.5 \times 10^{-3}$ pm^{-1} (r_{eff} > 2.2 Å) shown in Fig. 2c suggests that, for the larger cations, the interfacial capacitance is dominated by that of the region between then end of the gap and the OHP, *i.e.*, $\frac{1}{C_w} \gg \frac{1}{C_a} + \frac{1}{C_g}$ (see Eq. 2). As r_{eff} decreases, the contribution of the other two regions to the total capacitance and the overall potential drop become non-negligible, resulting in a deviation from the direct proportionality between C_T and $\frac{z}{r_H}$.

According to Eqs. 2 and 3, exactly the same dependence on $\frac{z}{r_H}$ should be expected for the STR and C_T, and the STR should be directly proportional to C_T if ε_a remains constant. Such behaviour would imply a rather expectable cation-dependent polarisation of CO_{ad}, sufficient to explain the trend observed with the largest cations. However, the deviation from a direct proportionality with $\frac{z}{r_H}$ for r_{eff} < 2.2 Å is stronger for the STR (Fig. 2c) than for C_T (Fig. 2d), which leads to the lack of direct proportionality between STR and C_T for cations smaller than TEA^+ observed in Fig. 2b. Assuming, in a first approximation, that $\frac{\partial \bar{\nu}_{CO_L}}{\partial F}$ is a constant, the deviation from a direct proportionality is only possible if, for sufficiently small cations, ε_a becomes cation dependent. *I.e.*, the small distance between the OHP and the electrode surface must provoke too large an electric field across CO_{ad}, to which it reacts with an increase of its polarizability (note that $\varepsilon = 1 + \chi$, where χ is the polarizability), which results in an electric field across CO_{ad} smaller than it would have been had the polarizability not increased. An increase in ε_a must lead to a stronger deviation from a direct proportionality with $\frac{z}{r_H}$ for the STR, because, while increasing ε_a affects both the numerator and the denominator of C_T, it

affects only the denominator of the STR. Actually, the higher sensitivity of the STR to changes in ε_a was to be expected, as capacitance measurements probe the whole interface, while $\frac{\partial \bar{\nu}_{CO_L}}{\partial \Delta\phi}$ probes only the CO adlayer and must therefore be more sensitive to variations in its properties.

3.2. Hydrogen bonding between interfacial water and CO_{ad}. At E < pzc, the interfacial water layer approaches closer to the surface and orientates itself with H pointing towards the surface (Fig. 3a, c and d). This will favour formation of hydrogen bonds with CO_{ad}, as confirmed by AIMD (Fig. 3e). The O-H stretching region of our spectra provides evidence of increased hydrogen bonding between interfacial water and CO_{ad} at increasingly negative potentials, as discussed below.

The spectra with H^+, NH_4^+, the alkaline-metal cations, Mg^{2+}, Ca^{2+} and Sr^{2+} (see Fig. 1d and Fig. S1b) are consistent with Yamakata's and Osawa's [38–40], who used CO-covered Pt electrodes and ATR-SEIRAS to study the hydration shell of several hydrophilic and hydrophobic cations. The spectra are dominated by positive bands at ~3600 cm^{-1}, corresponding to the O-H stretching of water molecules in the hydration shell of hydrophilic cations [38,39]. The lower frequency and broader bands observed in the case of NR_4^+ [38–40] (not shown in Fig. 1Sb) is evidence that hydrogen bonding within their solvation shells is stronger [38,39]. The relatively sharp negative band at 3670 cm^{-1} in Fig. 1d and Fig. S1b is characteristic of water with a low degree of hydrogen bonding, and has been assigned to the OH stretching of water molecules at the interface between hydrophobic CO-covered Pt and the electrolyte [41–43]. It is accompanied by a positive band around 3650 cm^{-1} that Yamakata and Osawa [39] have attributed to a red-shift of the band at 3670 cm^{-1}, due to the approach of the hydrated cations, resulting in a bipolar band that grows with increasing negative potential. Although we agree that this band is indeed due to a red-shift of the 3670 cm^{-1} band, we suggest instead that such shift is due to the increased hydrogen-down orientation of

interfacial water (Figs. 3c and d) and the resulting increased degree of hydrogen bonding with CO_{ad} (Fig. 3e).

Figs. 2c and d suggest that the cations' primary hydration shell is retained at the electrochemical double layer, at least at E > -0.1 V. The corresponding band about 3600 cm^{-1} red-shifts with increasing negative potentials (Fig. S4), providing evidence of increased polarisation of solvation water. (This band and this effect are not observed with NR_4^+, for this reason and for the sake of clarity, these cations were not included in Fig. S1b.) However, both its frequency and its shift with potential are cation independent (Fig. S4), *i.e.*, any cation effect on the degree of polarisation or on how much that polarisation increases with increasing negative potential is too small to be detected.

3.3 Relevance for the CO_2RR. Although the intense electric field at the EDL has been previously proposed as responsible for the remarkable cation sensitivity of both the activity and selectivity of the CO_2RR [14,44–46], ours is the first direct experimental evidence that field-induced effects go beyond increasing the degree of polarisation of adsorbed species. With sufficiently small cations, the close proximity of the OHP to the electrode surface generates an electric field across CO_{ad} intense enough to lead to a rearrangement of its electronic density large enough to result in an increased polarizability, the degree of which is cation dependent. This must have an effect on the adsorption energy of CO_{ad} (a critical reaction intermediate in the path to both C_1 and C_2 hydrogenated products) much stronger than that resulting from a simple increase in its polarisation. Other reaction intermediates, such as adsorbed OCCO and OCCOH, can also be affected by this kind of effects. Altogether, this must have a considerable impact on the apparent activation barriers of the different possible pathways. Although our work has focused on saturated CO adlayers on Pt, there is experimental evidence that the effects reported here are also at work for CO on Cu electrodes [33], probably the most studied material for CO_2 reduction.

Our spectra (Fig. 1d and Fig. S1b) and those in previous work [38–40] in the O-H stretching region, show evidence of increased hydrogen bonding at increasing negative potentials. Combined with the clear cation dependence of C_T (Fig. 2c), and because the charge density at a given potential will be larger the larger C_T, and so will be the degree of dipole orientation, we can conclude that the cation-dependent intensity of the electric field at the EDL must lead to a cation-dependent degree of hydrogen bonding of interfacial water with CO_{ad}, which contributes to the effect of cations on the CO_2RR, as recently suggested [15]. Although we have not found direct evidence in this work of differences in the degree of polarisation of solvation water for different cations, this might simply mean that the effect is too small to be detected spectroscopically. However, previous evidence from our own group [5] is strong enough to suggest that the cation-dependent intensity of the electric field at the EDL leads to a cation-dependent buffering capacity at the interface, which also contributes to the cation effect on the CO_2RR.

4. Conclusions

A detailed analysis of the correlation between C_T and the STR, and of each one of these magnitudes with $\frac{z}{r_H}$, combined with AIMD simulations, allows to formulate a detailed EDL model, in which the size of the hydrated cation determines the location of the OHP, which, for the same potential drop across the interface, results in a cation-dependent intensity of the interfacial electric field. The most relevant consequences of this are:

1. A cation dependent effective potential at the plane where the electron transfer happens, as recognised in early work [8]. This will affect the apparent activation energy of the overall reaction and, through it, its activity. It will also affect the activation energy of each individual step involving an electron transfer, including those determining the rates of parallel paths, and will also have, therefore, an effect on the reaction selectivity and on how it varies with potential.

2. A cation-dependent reorganisation of the electronic density of adsorbates. Depending on the cation and the adsorbate, this might result in a simple cation-dependent polarisation or have a stronger effect and lead to a change in the adsorbate's polarizability, as shown here for the case of CO_{ad} and cations smaller than TEA^+. If the electric field-induced reorganisation of electronic density is different for different adsorbed intermediates this will affect their adsorption energy in different degrees and will lead to a change in the apparent activation energy of the different possible paths.
3. As the pzc should, in principle, not be affected by the cation, smaller cations that result in larger C_T will lead to a larger negative charge density at the same applied potential, E (as far as E < pzc). This will result in a cation-dependent degree of orientation of interfacial water dipoles and, consequently, to differences in the degree of hydrogen bonding of interfacial water with adsorbed intermediates. In the particular case of CO_{ad}, this will, furthermore, be enhanced by the accumulation of electronic density on the oxygen atom resulting from the reorganisation of electronic density described in the preceding paragraph. As hydrogen bonding to adsorbed intermediates can play an important role in hydrogenation reactions, this must play a role in determining the activity and selectivity of these reactions.
4. The more intense interfacial electric fields with smaller cations will also result in a higher polarisation of their solvation shells, which will lead to differences in the pK_a of cation hydrolysis at the interface. In good agreement with this assertion, recently reported results [5] show that precisely those cations which have been shown here to have a smaller effective radius in aqueous electrolytes have a higher buffering capacity at the interface during the CO_2RR in CO_2-bicarbonate buffer solutions.

All these effects contribute to the sensitivity of the activity and selectivity of the CO_2RR to the electrolyte cation and reinforce each other, providing a comprehensive explanation to

previous results [4,5,14,15]. The question is, therefore, not which of them is responsible for the observed trends, but to which extent each one of them is determining those trends, and how they can be controlled to improve the activity and yield the desired product distribution.

Acknowledgements

The continuous support of the University of Aberdeen and financial support from the Leverhulme Trust through Research Grant RPG-2015-040 is gratefully acknowledged. A.C. and G.H. acknowledge the support of Universities UK international (UUKi) and the Department for Business, Energy & Industrial Strategy (BEIS) for a Rutherford Strategic Partner Grant (RF-2018-79) and a Rutherford Fellowship, respectively. J.C. is grateful for the financial support by the National Natural Science Foundation of China (Grants Nos. 2181101075 and 21621091), and J.L. thanks the China Postdoctoral Science Foundation (2018M642563) for support.

REFERENCES

[1] K.A. Schwarz, R. Sundararaman, T.P. Moffat, T.C. Allison, Formic acid oxidation on platinum: a simple mechanistic study, Phys. Chem. Chem. Phys. 17 (2015) 20805–20813.

[2] L.D. Chen, M. Urushihara, K. Chan, J.K. Nørskov, Electric Field Effects in Electrochemical CO_2 Reduction, ACS Catal. 6 (2016) 7133–7139.

[3] H. Xiao, T. Cheng, W.A. Goddard, R. Sundararaman, Mechanistic Explanation of the pH Dependence and Onset Potentials for Hydrocarbon Products from Electrochemical Reduction of CO on Cu (111), J. Am. Chem. Soc. 138 (2016) 483–486.

[4] M.R. Singh, Y. Kwon, Y. Lum, J.W. Ager, A.T. Bell, Hydrolysis of Electrolyte Cations Enhances the Electrochemical Reduction of CO_2 over Ag and Cu, J. Am. Chem. Soc. 138 (2016) 13006–13012.

[5] O. Ayemoba, A. Cuesta, Spectroscopic Evidence of Size-Dependent Buffering of

Interfacial pH by Cation Hydrolysis during CO_2 Electroreduction, ACS Appl. Mater. Interfaces. 9 (2017) 27377–27382.

[6] A. Murata, Y. Hori, Product Selectivity Affected by Cationic Species in Electrochemical Reduction of CO_2 and CO at a Cu Electrode, Bull. Chem. Soc. Jpn. 64 (1991) 123–127.

[7] A.N. Frumkin, Wasserstoffuberspannung und Struktur der Doppelschicht, Z. Phys. Chem. 164 (1933) 121.

[8] W.R. Fawcett, The effect of ionic size in the double layer on the kinetics of electrode reactions, J. Electroanal. Chem. 22 (1969) 19–28.

[9] W.R. Fawcett, Examination of the role of ion size in determining double layer properties on the basis of a generalized mean spherical approximation, J. Electroanal. Chem. 500 (2001) 264–269.

[10] R.R. Nazmutdinov, D. V. Glukhov, G.A. Tsirlina, O.A. Petrii, Exploring the molecular features of cationic catalysis phenomenon: Peroxodisulfate reduction at a mercury electrode, J. Electroanal. Chem. 582 (2005) 118–129.

[11] Y. Hori, A. Murata, R. Takahashi, Formation of hydrocarbons in the electrochemical reduction of carbon dioxide at a copper electrode in aqueous solution, J. Chem. Soc. Faraday Trans. 1 85 (1989) 2309–2326.

[12] C.W. Li, J. Ciston, M.W. Kanan, Electroreduction of carbon monoxide to liquid fuel on oxide-derived nanocrystalline copper, Nature. 508 (2014) 504–507.

[13] X. Feng, K. Jiang, S. Fan, M.W. Kanan, A Direct Grain-Boundary-Activity Correlation for CO Electroreduction on Cu Nanoparticles, ACS Cent. Sci. 2 (2016) 169–174.

[14] E. Pérez-Gallent, G. Marcandalli, M.C. Figueiredo, F. Calle-Vallejo, M.T.M. Koper, Structure- and Potential-Dependent Cation Effects on CO Reduction at Copper Single-

Crystal Electrodes, J. Am. Chem. Soc. 139 (2017) 16412–16419.

[15] J. Li, X. Li, C.M. Gunathunge, M.M. Waegele, Hydrogen bonding steers the product selectivity of electrocatalytic CO reduction., Proc. Natl. Acad. Sci. 116 (2019) 9220–9229.

[16] J.D. Roth, M.J. Weaver, Role of double-layer cation on the potential-dependent stretching frequencies and binding geometries of carbon monoxide at platinum-nonaqueous interfaces, Langmuir. 8 (1992) 1451–1458.

[17] A. López-Cudero, A. Cuesta, C. Gutiérrez, The effect of chloride on the electrooxidation of adsorbed CO on polycrystalline platinum electrodes, J. Electroanal. Chem. 548 (2003) 109–119.

[18] A. Cuesta, Measurement of the surface charge density of CO-saturated Pt(111) electrodes as a function of potential: The potential of zero charge of Pt(111), Surf. Sci. 572 (2004) 11–22.

[19] S. Baldelli, Probing Electric Fields at the Ionic Liquid−Electrode Interface Using Sum Frequency Generation Spectroscopy and Electrochemistry, J. Phys. Chem. B. 109 (2005) 13049–13051.

[20] A. López-Cudero, A. Cuesta, C. Gutiérrez, Potential dependence of the saturation CO coverage of Pt electrodes: The origin of the pre-peak in CO-stripping voltammograms. Part 1: Pt(111), J. Electroanal. Chem. 579 (2005) 1–12.

[21] A. López-Cudero, Á. Cuesta, C. Gutiérrez, Potential dependence of the saturation CO coverage of Pt electrodes: The origin of the pre-peak in CO-stripping voltammograms. Part 2: Pt(100), J. Electroanal. Chem. 586 (2006) 204–216.

[22] A. Cuesta, A. Couto, A. Rincón, M.C. Pérez, A. López-Cudero, C. Gutiérrez, Potential dependence of the saturation CO coverage of Pt electrodes: The origin of the pre-peak in CO-stripping voltammograms. Part 3: Pt(poly), J. Electroanal. Chem. 586 (2006)

184–195.

[23] R. Sundararaman, M.C. Figueiredo, M.T.M. Koper, K.A. Schwarz, Electrochemical Capacitance of CO-Terminated Pt(111) Dominated by the CO–Solvent Gap, J. Phys. Chem. Lett. 8 (2017) 5344–5348.

[24] M.C. Figueiredo, D. Hiltrop, R. Sundararaman, K.A. Schwarz, M.T.M. Koper, Absence of diffuse double layer effect on the vibrational properties and oxidation of chemisorbed carbon monoxide on a Pt(111) electrode, Electrochim. Acta. 281 (2018) 127–132.

[25] K.P. Kuhl, E.R. Cave, D.N. Abram, T.F. Jaramillo, New insights into the electrochemical reduction of carbon dioxide on metallic copper surfaces, Energy Environ. Sci. 5 (2012) 7050–7059.

[26] A.M. Appel, J.E. Bercaw, A.B. Bocarsly, H. Dobbek, D.L. DuBois, M. Dupuis, J.G. Ferry, E. Fujita, R. Hille, P.J.A. Kenis, C.A. Kerfeld, R.H. Morris, C.H.F. Peden, A.R. Portis, S.W. Ragsdale, T.B. Rauchfuss, J.N.H. Reek, L.C. Seefeldt, R.K. Thauer, G.L. Waldrop, Frontiers, Opportunities, and Challenges in Biochemical and Chemical Catalysis of CO_2 Fixation, Chem. Rev. 113 (2013) 6621–6658.

[27] J.D. Goodpaster, A.T. Bell, M. Head-Gordon, Identification of Possible Pathways for C–C Bond Formation during Electrochemical Reduction of CO_2: New Theoretical Insights from an Improved Electrochemical Model, J. Phys. Chem. Lett. 7 (2016) 1471–1477.

[28] A. Miki, S. Ye, M. Osawa, Surface-enhanced IR absorption on platinum nanoparticles: an application to real-time monitoring of electrocatalytic reactions, Chem. Commun. (2002) 1500–1501.

[29] M. Osawa, In-situ Surface-Enhanced Infrared Spectroscopy of the Electrode/Solution Interface, in: R.C. Alkire, D.M. Kolb, J. Lipkowsky, P.N. Ross (Eds.), Advances in

Electrochemical Science and Engineering, John Wiley & Sons, Ltd, Weinheim, Germany, Vol. 9, 2008: pp. 269–314.

[30] R. Kas, O. Ayemoba, N.J. Firet, J. Middelkoop, W.A. Smith, A. Cuesta, In-Situ Infrared Spectroscopy Applied to the Study of the Electrocatalytic Reduction of CO_2 : Theory, Practice and Challenges, ChemPhysChem. doi:10.1002/cphc.201900533.

[31] J. Le, M. Iannuzzi, A. Cuesta, J. Cheng, Determining Potentials of Zero Charge of Metal Electrodes versus the Standard Hydrogen Electrode from Density-Functional-Theory-Based Molecular Dynamics, Phys. Rev. Lett. 119 (2017) 016801.

[32] I. Villegas, M.J. Weaver, Carbon monoxide adlayer structures on platinum (111) electrodes: A synergy between in-situ scanning tunneling microscopy and infrared spectroscopy, J. Chem. Phys. 101 (1994) 1648–1660.

[33] C.M. Gunathunge, V.J. Ovalle, M.M. Waegele, Probing promoting effects of alkali cations on the reduction of CO at the aqueous electrolyte/copper interface, Phys. Chem. Chem. Phys. 19 (2017) 30166–30172.

[34] K. Kunimatsu, W.G. Golden, H. Seki, M.R. Philpott, Carbon Monoxide Adsorption on a Platinum Electrode Studied by Polarization Modulated FT-IRRAS. 1. CO Adsorbed in the Double-Layer Potential Region and Its Oxidation in Acids, Langmuir. 1 (1985) 245–250.

[35] N. Agmon, The Grotthuss mechanism, Chem. Phys. Lett. 244 (1995) 456–462.

[36] S.-C. Chang, M.J. Weaver, Coverage- and potential-dependent binding geometries of carbon monoxide at ordered low-index platinum- and rhodium-aqueous interfaces: comparisons with adsorption in corresponding metal-vacuum environments, Surf. Sci. 238 (1990) 142–162.

[37] L.W.H. Leung, A. Wieckowski, M.J. Weaver, In situ infrared spectroscopy of well-defined single-crystal electrodes: adsorption and electrooxidation of carbon monoxide

on platinum(111), J. Phys. Chem. 92 (1988) 6985–6990.

[38] A. Yamakata, M. Osawa, Destruction of the Water Layer on a Hydrophobic Surface Induced by the Forced Approach of Hydrophilic and Hydrophobic Cations, J. Phys. Chem. Lett. 1 (2010) 1487–1491.

[39] A. Yamakata, M. Osawa, Cation-dependent restructure of the electric double layer on CO-covered Pt electrodes: Difference between hydrophilic and hydrophobic cations, J. Electroanal. Chem. 800 (2017) 19–24.

[40] A. Yamakata, M. Osawa, Destruction of the Hydration Shell around Tetraalkylammonium Ions at the Electrochemical Interface, J. Am. Chem. Soc. 131 (2009) 6892–6893.

[41] M. Osawa, M. Tsushima, H. Mogami, G. Samjeske, A. Yamakata, Structure of Water at the Electrified Platinum−Water Interface: A Study by Surface-Enhanced Infrared Absorption Spectroscopy, J. Phys. Chem. C. 112 (2008) 4248–4256.

[42] A. Cuesta, Comments on the paper by H. Shiroishi, Y. Ayato, K. Kunimatsu and T. Okada entitled “Study of adsorbed water on Pt during methanol oxidation by ATR-SEIRAS (surface-enhanced infrared absorption spectroscopy)” [J. Electroanal. Chem. 581 (2005) 132], J. Electroanal. Chem. 587 (2006) 329–330.

[43] J.A. Santana, Y. Ishikawa, Density-functional theory study of interactions between water and carbon monoxide adsorbed on platinum under electrochemical conditions, Chem. Phys. Lett. 478 (2009) 110–114.

[44] S.A. Akhade, I.T. McCrum, M.J. Janik, The Impact of Specifically Adsorbed Ions on the Copper-Catalyzed Electroreduction of CO_2, J. Electrochem. Soc. 163 (2016) F477–F484.

[45] R.B. Sandberg, J.H. Montoya, K. Chan, J.K. Nørskov, CO-CO coupling on Cu facets: Coverage, strain and field effects, Surf. Sci. 654 (2016) 56–62.

[46] L.D. Chen, M. Urushihara, K. Chan, J.K. Nørskov, Electric Field Effects in Electrochemical CO_2 Reduction, ACS Catal. 6 (2016) 7133–7139.